ACS APPLIED MATERIALS & INTERFACES

Research Article

www.acsami.org

Glass–NiP–CoFeP Triplex-Shell Particles with Hollow Cores and Tunable Magnetic Properties

Zhenguo An* and Jingjie Zhang*

Technical Institute of Physics and Chemistry, Chinese Academy of Sciences, Beijing, 100190 China

Supporting Information

ABSTRACT: Low density (0.55–0.92g/mL, depending on the shell thickness and composition) glass–metal–metal triplex-shell hollow particles (TSHP) were prepared by a three-step route. First, micrometer-sized silicate glass particles with hollow cores, uniform shells, and high sphericity were prepared through spray drying and subsequent melting. NiP shell was uniformly assembled to the previously obtained glass hollow particles by silver seed induced chemical reduction of Ni^{2+} by sodium hypophosphite, and glass–NiP double-shell hollow particles (DSHP) with compact and uniform shells were formed. The as-formed NiP particles further acted as the seeds for the directed formation and assembly of the CoFeP shell on the NiP shell to form the final glass–NiP–CoFeP triplex-shell hollow particles (TSHP). The influences of the component of the reaction system on the composition, structure, and magnetic properties of the hollow particles were studied. The multishell hollow particles thus obtained may have some promising applications in the fields of low-density magnetic materials, conduction, microwave absorbers, catalysis, etc. This work provides an additional strategy to fabricate multishell structured hollow particles with tailored shell composition and magnetic properties, which can be extended to the controlled preparation of multishell composite particles with the shells consisting of metal, oxides, or other compounds.

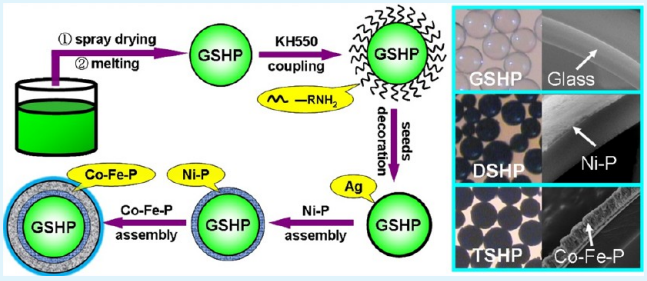

KEYWORDS: *hollow particles, controlled assembly, triplex-shell, magnetic properties*

1. INTRODUCTION

In the past decades, the design, preparation, and modification of hollow particles on micrometer, submicrometer, or nanometer scale have attracted considerable attention, for the hollow structure usually endows these hollow particles unique properties and wide application potential in various fields such as chemical reactors, drug delivery, sensors, catalysis, lightweight functional stuffs, and so on.[1−4] In particular, composite hollow particles with multishell structure fabricated by the hierarchical assembly of building units with heterogeneous phases at different levels is one of the important forms among these hollow structured particles. The multishell structure can bring the hollow particles new or improved behaviors in addition to those arisen from their hollow cores and hence are potentially useful in a much broader field of application. Moreover, the application demand on functional materials increasingly tend to multifunctionalization and property enhancement; to meet these demands, multishell structure is a promising candidate, because through shell combination, improved and easy-tailored properties can be expected by properly tailoring the composition, morphology, and structure of the shells.[5−7] However, the fabrication of multishell hierarchical structures and fine control over their properties are still currently considerably difficult. To further understand the growth mechanism of heterogeneous multishell structures and study their composition and structure-dependent properties, hierarchical multishell structures need to be explored in more detail.

Generally, there are two strategies commonly employed for the manufacture of hollow materials: template assisted preparation (e.g., layer-by-layer deposition of low size level particles onto colloids and sacrificial substitutions of metal particles by those with a higher standard reduction potential) and template-free preparation (e.g., utilization of some physical phenomena, such as the Kirkendall effect, Ostwald ripening, self-assembly, etc.).[8−11] For the template directed synthesis, the advantage lies in that the size, shell thickness, and composition of the hollow structures thus obtained can be easily tailored by properly choosing the templates and the reaction condition, but to remove the templates, time-consuming post-treatment such as calcination or dissolution with solvent is needed, which usually leads to composition and structure variation of the shells. Moreover, the shells are relatively loose, and the hollow structure is not stable, which usually leads to low mechanical strength and poor performance in application. The Kirkendall effect and Ostwald ripening are more suitable for the hollowing of nanosized particles and, similar to template directed synthesis, they are difficult to be applied to large scale

Received: November 8, 2012
Accepted: January 2, 2013
Published: January 2, 2013

Table 1. Detailed Reagent Concentrations in the Reaction System and the Reaction Conditions for Different Samples

	reagent concentrations (g/L) and reaction conditions for different samples						
reagents and factors	S0	S1	S2	S3	S4	S5	S6
$NiSO_4{\cdot}6H_2O$	60						
$NaH_2PO_2{\cdot}H_2O$	25	30	30	30	30	30	30
$CoSO_4{\cdot}7H_2O$		25.8	23.1	20	17.7	14.9	12.2
$(NH_4)_2Fe(SO_4)_2{\cdot}6H_2O$		1.9	5.7	10	13.3	17.7	20.9
$(NH_4)_2SO_4$	40	40	40	40	40	40	40
$KNaC_4H_4O_6{\cdot}2H_2O$	80	60	60	60	60	60	60
pH value	9.5	9.0	9.0	9.0	9.0	9.0	9.0
temperature/°C	70	80	80	80	80	80	80
mole ratio $(Fe^{2+}/(Co^{2+} + Fe^{2+}))$		0.05	0.15	0.25	0.35	0.45	0.55

preparation. On the other hand, for the formation of multishell structures, one may employ the fabrication strategies of core−shell structures, on which remarkable progresses have been reported in the past decades.[5,12,13] The major precondition is that the first shell with hollow core must be of enough strength and stability; thus, the hollow structure and the first shell can be kept still during the directed assembly of the subsequent shells, which may involve multistep reactions and pre- or post-treatments.

Herein, we report a facile and reliable method for the controlled preparation of glass−metal−metal triplex-shell hollow particles (hereinafter referred to as TSHP for short) with silicate glass as the first shell by a three-step route. The formation of the hollow core, assembly of different shells, and control over the magnetic properties were all studied. The glass shells are prepared through a two step spray drying−smelting method. These hollow particles with glass shells (hereinafter referred to as GSHP for short) further act as "hollow cores" for the directed chemical reduction of Ni^{2+} by sodium hypophosphite (silver seed induced) to obtain glass−NiP double-shell hollow particles (hereinafter referred to as DSHP for short). Subsequently, the as-formed NiP particles further acted as the seeds for the reduction and directed assembly of Co^{2+} and Fe^{2+} to form CoFeP shells on the NiP shells, and finally, glass−NiP−CoFeP TSHP were prepared. The effects of the component of the reaction solution and the reaction conditions on the composition, structure, and the magnetic properties of the as-obtained multishell particles were studied. The multishell structured particles with hollow core can combine the advantages of low density and easy-tailored magnetic behavior, and a wider application field is promising.

2. EXPERIMENTAL SECTION

2.1. Synthesis. All reagents were of analytical grade and used without further purification. The hollow microspheres with glass shell were synthesized through a two-step spray drying (first step)−smelting (second step) method. A slurry was made consisting of 100 g of SiO_2 (silica hydrated), 10 g of CaO, 10 g of Na_2SO_4, 15 g of Na_2CO_3, 1.0 g of polyethylene oxide, and 12 g of H_3BO_3 in 400 mL of deionized water and stirred vigorously for 3.0 h. Then, the slurry was milled in a colloid mill for 5 h and, subsequently, spry dried with a nozzle inlet temperature of 300 °C and a feeding rate of 15 mL/min. Quasi spherical precursor particles were obtained caused by evaporation of the solvent and surface tension and collected by a cyclone separator. The precursor particles were then immediately introduced into a natural gas/air torch to get spherical glass shells with hollow cores and smooth surface. In the smelting process, the precursor particles encountered the flame and were further sphericized due to the high flame temperature and surface tension of the glass melt.[14,15]

Before the assembly of the NiP shell (on the glass shell), the hollow particles with glass shells underwent a coupling process (in 30 g/L 3-aminopropyltriethoxy silane ethanol solution, 60 °C for 30 min; then, the microspheres were filtered off and dried in a vacuum drying chamber at 120 °C for 2.0 h) and, subsequentially, a sensitization (in a solution containing 15 g/L $SnCl_2$ and 5 mL/L HCl, at room temperature for 10 min) and activation process (2.0 g of the microspheres gained from the coupling step were dispersed in 150 mL of a solution containing 20 g/L $AgNO_3$ and 15 mL/L ammonia (25%) at room temperature for 20 min) to decorate the glass shell surface with Ag^+. The activated microspheres were separated, washed twice with deionized water, and put in vacuum drying chamber at 60 °C. The assembly of the NiP shell on the glass shell was carried out in an alkaline solution of the following composition: $NiSO_4{\cdot}6H_2O$, 60 g/L; $NaH_2PO_2{\cdot}H_2O$, 25g/L; $KNaC_4H_4O_6{\cdot}2H_2O$, 80g/L; $(NH_4)_2SO_4$, 40 g/L. The pH value of the reaction solution was 9.5 (adjusted by ammonia); the reaction temperature and time were 70 °C and 20 min, respectively (sample S0 in Table 1). The as-formed NiP shell further acted as the "seed" for the directed formation and assembly of CoFeP particles to form the third shell, which was carried out in an alkaline solution (the composition of the reaction system and the reaction condition for different samples are listed in Table 1). Six samples were prepared with the same glass and NiP shells but different CoFeP shell (S1−S6 in Table 1) to study the influence of the mole ratio of $(Fe^{2+}/(Co^{2+} + Fe^{2+}))$ on the composition, structure, and magnetic properties of the TSHP. After reaction, the products were separated from the solution by vacuum filtration, rinsed thrice with deionized water, and dried at 60 °C in a vacuum drying chamber.

2.2. Characterization. The scanning electron microscopy (SEM) images and energy dispersive X-ray (EDX) spectrum of the hollow particles at different stages were obtained using a Hitachi S-4300 microscope and EMAX Horiba, respectively. To prevent surface charging, the samples were covered for SEM with a thin layer of Au before observation. The optical microscopy images of the products were obtained using an AxioImager.A2m optical microscope. The real densities of the hollow particles at different stages were measured by an AccuPyc II 1340 gas displacement pycnometry system with N_2 as the working gas. A MGU15-75DC compressive resistance tester was used for the isopressing treatment of the GSHP. Because the breaking of a hollow particle can lead to density variety, the densities of the initial GSHP, the isopressing treated GSHP, and the broken GSHP were measured for the calculation of the broken ratio (σ) of the GSHP after isopressing treatment at a certain pressure. The theoretical derivation process and the final formula for the calculation of the σ of the GSHP were listed below. The structures of the as-obtained products were studied by X-ray diffraction (XRD, D/max 2200 PC, Rigaku, Japan) with a Cu target radiation (λ = 0.15406 nm) in the 2θ ranging from 10° to 80°. The magnetic measurements of the products were performed at room temperature using a vibrating sample magnetometer (VSM, Lake Shore 7307).

Calculation of the Broken Ratio (σ) of the GSHP. It is known that the weight of the GSHP before and after isopressing treatment is constant, so we can get Formula 1, where V_b and ρ_b represent the volume and density of the GSHP before isopressing treatment and V_a

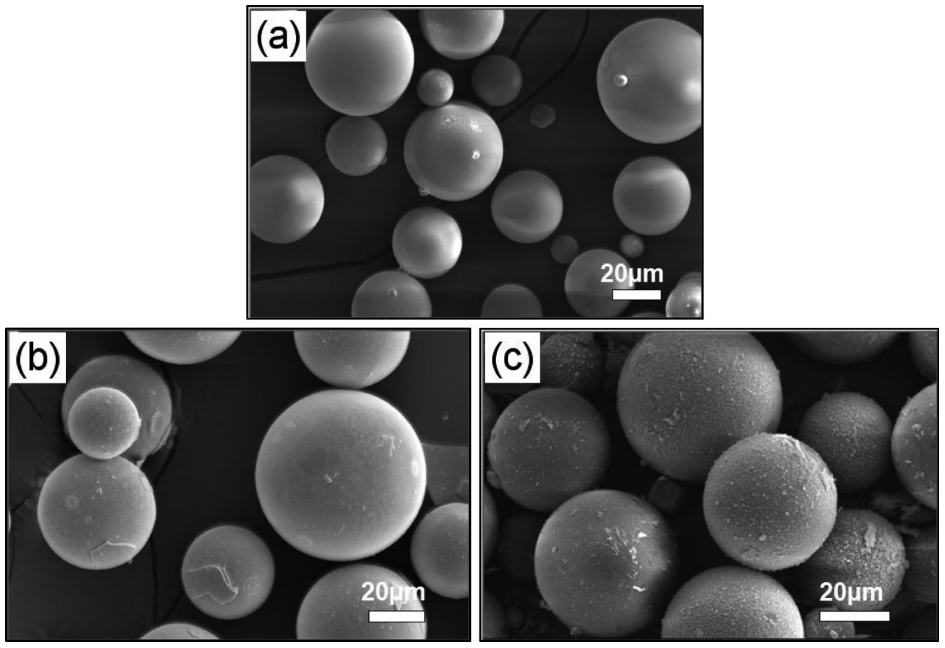

Figure 1. SEM images of the as-obtained GSHP (a), the glass−NiP DSHP (S0, b), and the glass−NiP−CoFeP TSHP (S3, c).

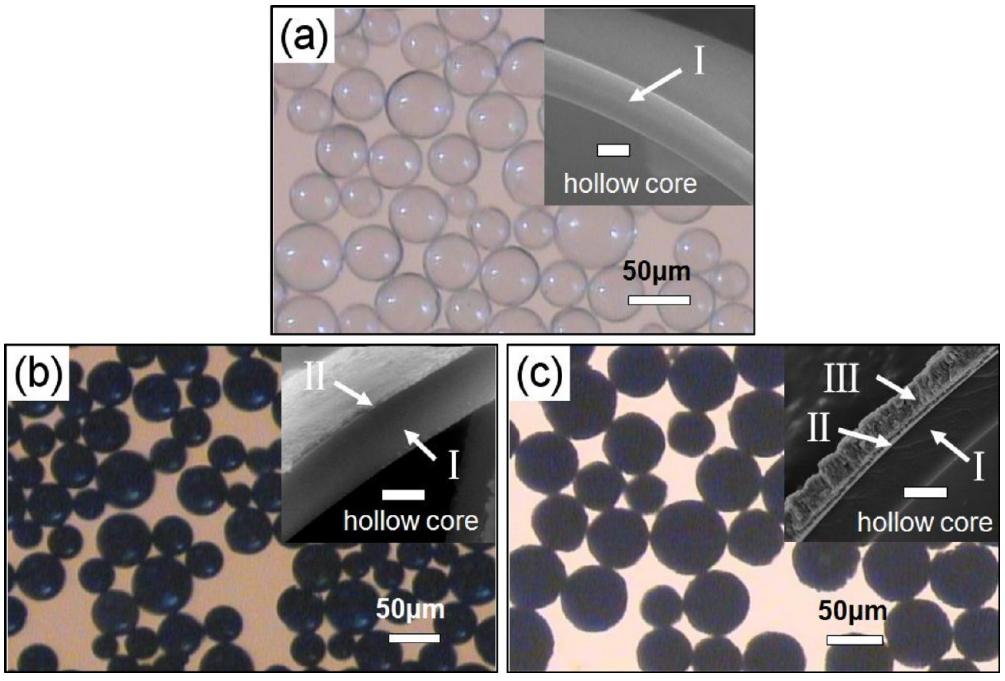

Figure 2. Optical microscopy images of the as-obtained GSHP (a), the glass−NiP DSHP (S0, b), and the glass−NiP−CoFeP TSHP (S3, c). The insets are the SEM images of the fragments of the corresponding particles, which illustrate the different shell structures of the three types of hollow particles. I, silicate glass shell; II, NiP shell; III, CoFeP shell. The scale bars in all the insets present 1 μm.

and ρ_a represent the volume and density of the GSHP after isopressing treatment, respectively. V_a can be given by Formula 2, where ρ_g stands for the density of broken GSHP. Taking Formulas 2 and 1, we can get Formula 3, from which the broken ratio (σ) can be calculated (Formula 4).

$$V_b/V_a = \rho_a/\rho_b \quad (1)$$

$$V_a = (1 - \sigma)V_b + \sigma V_b\rho_b/\rho_g \quad (2)$$

$$\rho_b\rho_a = 1 - \sigma((\rho_g - \rho_b)/\rho_g) \quad (3)$$

$$\sigma = \rho_g(\rho_a - \rho_b)/\rho_a(\rho_g - \rho_b) \quad (4)$$

3. RESULTS AND DISCUSSION

The morphologies of the hollow particles at different stages were studied with field emission scanning electron microscopy (FE-SEM) and optical microscopy, as shown in Figures 1 and 2. Figure 1a depicts a panoramic image of the GSHP, from which it can be seen that, after the two-step spraying drying (first step)−smelting (second step) reaction, micrometer-sized spherical particles were obtained with continuous and uniform

dx.doi.org/10.1021/am3026344 | ACS Appl. Mater. Interfaces 2013, 5, 989−996

shells. These particles possess a smooth surface and a diameter distribution range of 10−60 μm. The real density of the as-obtained GSHP was 0.30 g/mL. After isopressing treatment at 10 MPa, the real density increased to 0.33 g/mL, which can be attributed to the fact that the breaking of some hollow particles led to the decrease of the volume. As shown in Table 2, the real

Table 2. Densities and Broken Ratio of the As-Obtained GSHP after Isopressing Treatment at a Pressure of 10 MPa

ρ_b/g·mL^{-1}	ρ_a/g·mL^{-1}	ρ_g/g·mL^{-1}	σ/%
0.30	0.33	2.55	10.30

density of the broken GSHP was measured to be 2.55, and the broken ratio of the GSHP can be calculated by Formula 4 as 10.30%. These results reveal that the as-obtained GSHP from our two-step method possess both low density and relatively high mechanical strength. Moreover, as a glass material, it can be expected that the GSHP will keep stable at many traditional reaction conditions and can be a promising candidate as lightweight cores for the preparation of composite hollow particles. After the assembly of the second shell (the NiP shell), as shown in Figure 1b, the surface of the particles became coarser, and some granular tubercles can be seen on the NiP shell. With the further assembly of the third shell (CoFeP shell), the surface of the particles gets increasingly coarse; many little granules can be seen attached on the CoFeP shell (Figure 1c).

Although the panoramic SEM images can give the information of the particle diameters and the approximate appearance of the products, they cannot verify the multishell hollow structure of the particles. To further reveal the hollow structure of the products and the status of different shells, optical microscopy images and SEM images of the fragments of the products at different stages with higher magnification were obtained. From the optical microscopy image of Figure 2a, it can be seen that the glass shell possesses high uniformity and transparency. The inset of Figure 2a is the SEM image of a fragment of the glass shell, which also confirms the smooth and compact nature of the glass shells (shell I, shell thickness, ca. 1.3 μm). Figure 2b reveals that, after the assembly of NiP shell (shell II), the as-obtained DSHP were no longer transparent. However, due to the relatively uniform and smooth shell surface, the DSHP still possess glossiness in some degree. The SEM image of a fragment of the DSHP (inset of panel b, Figure 2) indicates that the NiP shell attached compactly to the glass shell, and the thickness of the NiP shell is ca. 300 nm. Panel (c) in Figure 2 is the optical microscopy image of the final TSGP. It can be observed that, after the assembly of the CoFeP shell (shell III), the hollow particles got opaque and matte, which may be attributed to the coarse shell surface and high shell thickness (ca. 750 nm). The inset of panel (c) in Figure 2 was the SEM image of a fragment of the final TSHP, which gives a clear view of the final products (i.e., particles with glass−NiP−CoFeP triplex shells and hollow cores).

The stepwise fabrication process of the three shells and the final TSHP is schematically shown in Figure 3. In the two-step spraying drying−smelting part, the slurry was atomized by a centrifugal atomizer and the droplets thus obtained went into the drying chamber immediately, in which precursor particles were formed by evaporation of the solvent and surface tension. As shown in Figure S1, Supporting Information, the precursor particles were quasi spherical with a coarse and porous surface.

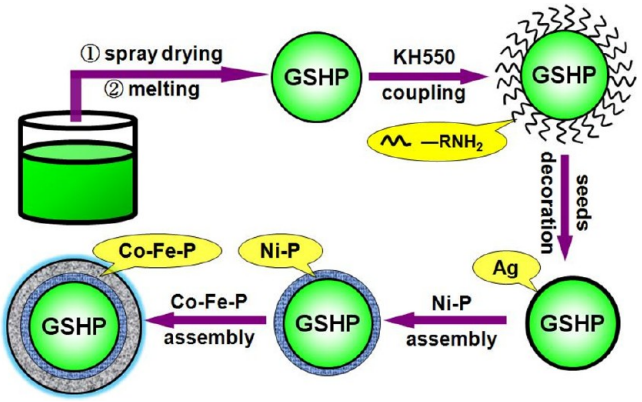

Figure 3. Schematic illustration of the formation process of the glass−NiP−CoFeP TSHP.

Then, after the smelting step, GSHP with compact and smooth surfaces were obtained (Figures 1a and 2a). Before the assembly of NiP shell on the GSHP, a pretreatment was carried out to make the glass shell active for the reduction of Ni^{2+}, which also involved two steps: coupling and activating. Here, relatively inexpensive silver ions were used as the activator, and 3-aminopropyltriethoxy silane (KH550) was employed as coupling agent to make the decoration of the glass shell by Ag^+ more efficient. The silver ions were reduced first in the reaction solution and further acted as catalytic active centers for the reduction of Ni^{2+} at the initial reaction stage in the process for NiP granule assembly, which ensures the directed assembly of the NiP shell onto the glass shell. In the attempts without coupling by KH550, NiP granules generated by the reduction of Ni^{2+} tend to aggregate to form irregular isolated micrometer particles instead of direct assembly on the GSHP to form uniform shells (Figure S2, Supporting Information). In the process for CoFeP shell assembly, the as-formed NiP shell further acted as the seed for the direct formation and assembly of CoFeP granules to form the third shell. A contrast experiment was carried out using the activated GSHP (without NiP shell) directly for the assembly of the CoFeP shell, and no reaction was observed with the equal reaction system component and reaction condition.

The stepwise synthesis of the TSHP was also confirmed by EDX and XRD analysis (Figures 4 and 5). Different kinds of EDX spectra were taken by passing the electron beam through different shells simultaneously and through only one shell region for the samples obtained at different reaction stages. Figure 4A is the EDX spectrum of the hollow particles obtained after the two-step spraying drying−smelting reaction, which shows the presence of Na, Ca, O, and Si in the glass shell. The corresponding XRD pattern of the product at this stage exhibits only a broad low diffraction peak, indicating the amorphous nature of the glass shell. For the DSHP obtained after NiP shell assembly, the EDX spectrum carried out by passing the electron beam through both shells simultaneously shows the presence of Ni, P, O, and Si, while the EDX spectrum obtained by passing the electron beam through only the outmost shell region indicates the existence of only Ni and P (see Figure 4B,C). Compared to the XRD pattern of the GSHP, an additional broad low diffraction peak appeared on the XRD pattern of the DSHP, which can be indexed to amorphous NiP alloy. On the other hand, the EDX spectrum of the TSHP obtained by passing the electron beam through only the outmost shell region indicates the existence of Co, Fe, and P, which confirms

dx.doi.org/10.1021/am3026344 | ACS Appl. Mater. Interfaces 2013, 5, 989−996

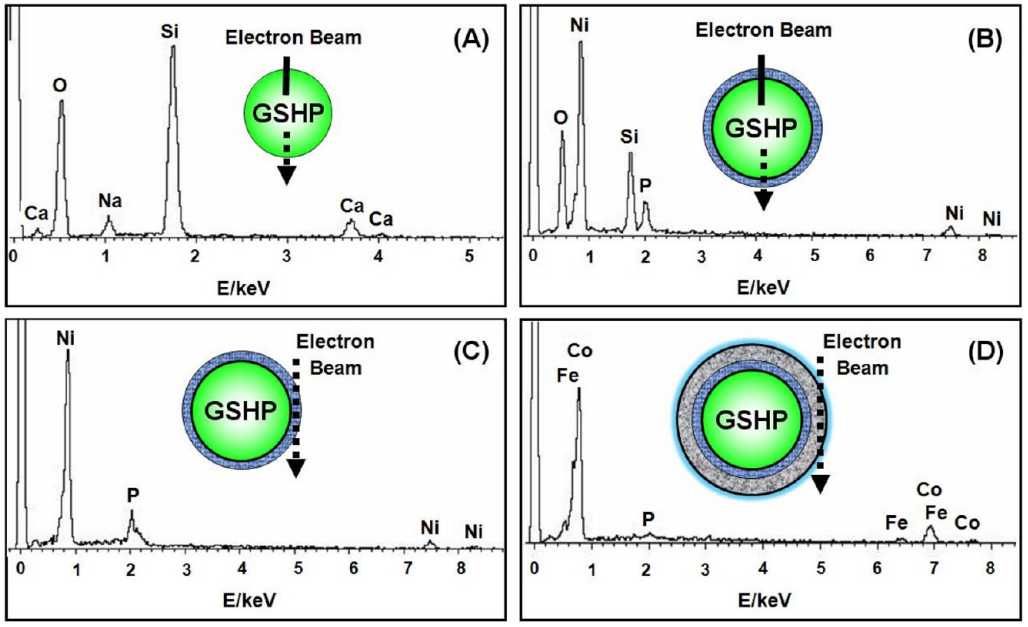

Figure 4. EDX spectra of the as-obtained GSHP (A), the DSHP taken by passing the beam through both shells (B) and only the outermost shell (C), and the TSHP taken by passing the beam through the outermost shell (D).

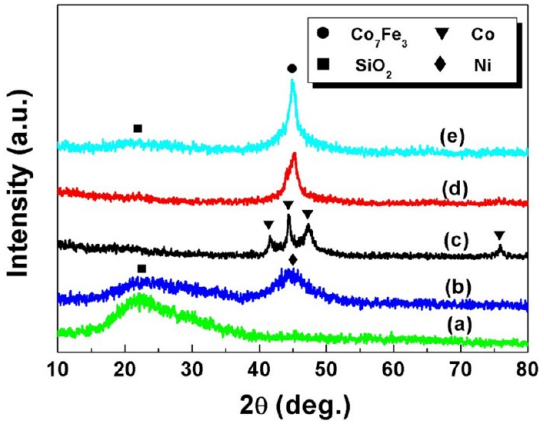

Figure 5. XRD patterns of the as-obtained GSHP (a), the glass−NiP DSHP (b), and the glass−NiP−CoFeP TSHP ((c): S1; (d): S3; (e): S6).

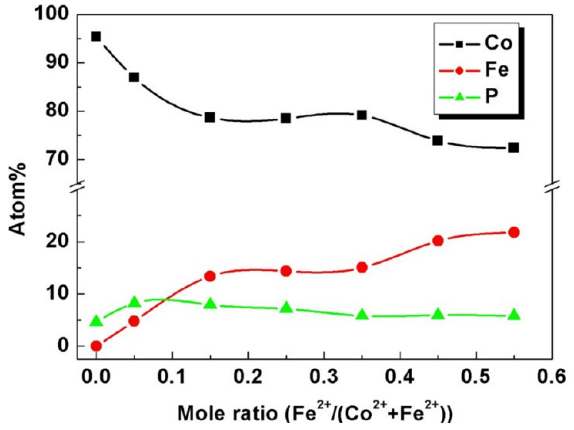

Figure 6. Changes of the composition of the Co−Fe−P shell at various mole ratios of Fe^{2+} ($Fe^{2+}/(Co^{2+} + Fe^{2+})$) in the reaction solution.

the formation of the CoFeP shell. The XRD patterns of S1, S3, and S6 are listed in Figure 5. It can be seen that, with low Fe^{2+} content in the reaction solution (S1), the diffraction peaks of metal Co were apparent (pattern (c) in Figure 5). When the Fe^{2+} content increased to 25 mol % (S3), the XRD patterns show the presence of CoFe alloy (pattern (d) in Figure 5), and the diffraction peaks get sharper with the further increased Fe^{2+} content (S6, pattern (d) in Figure 5).[16,17]

Figure 6 shows the effects of the mole ratios of $Fe^{2+}/(Co^{2+} + Fe^{2+})$ in the reaction system on the composition of the CoFeP shells (the atom ratios were obtained by EDX). It is found that the phosphorus content in the CoFeP shell was kept in a relatively low degree and changes slightly, and the iron and nickel contents in the CoFeP shell changed in an opposite sense. At lower mole ratio (0−0.15), the iron content in the CoFeP shell increased with the increased mole ratio in an approximate linear manner. However, when the mole ratios were above 0.25, the growth rate of the iron content in the CoFeP shell became lower, and the iron content in the CoFeP shell got increasingly lower than the Fe^{2+} content in the reaction system. This disproportionate iron content was also observed in NiFeP[18,19] and NiCoFeP[20] shells, which may be attributed to iron possibly possessing inferior catalytic activity than cobalt and nickel, and was more difficult to be formed in the reported condition. This was verified by the density variation of the TSHP: with the increased iron content, the reaction rate got lower and the densities of the as-obtained TSHP with identical reaction time and condition were reduced monotonically (see Table 3).

The magnetic properties of the hollow particles with different shell structures were studied in their as-obtained condition. The GSHP with noncrystalline silicate glass were nonmagnetic. After the direct assembly of the NiP shell, the as-obtained

Table 3. Real Densities of Different Samples

samples	S0	S1	S2	S3	S4	S5	S6
ρ_r/g·mL^{-1}	0.43	0.92	0.89	0.85	0.73	0.64	0.55

dx.doi.org/10.1021/am3026344 | ACS Appl. Mater. Interfaces 2013, 5, 989−996

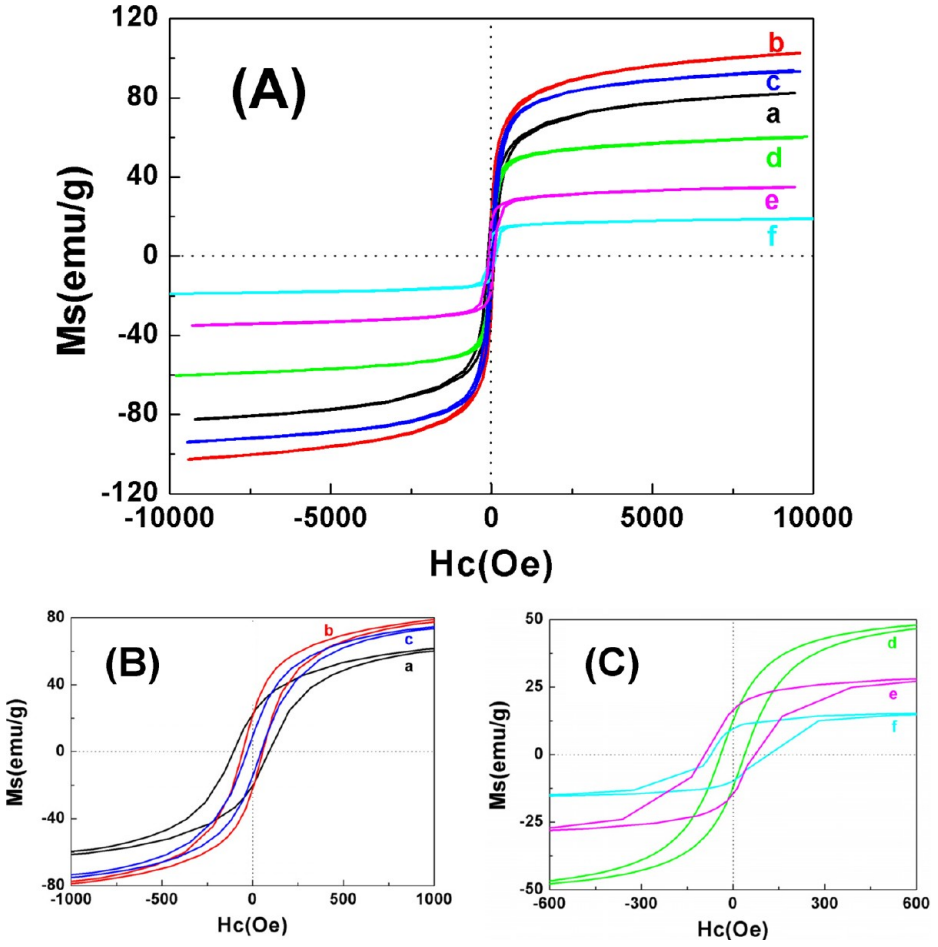

Figure 7. Field dependent magnetization at room temperature for the glass−NiP−CoFeP TSHP (panel (A): overall hysteretic loops; panels (B) and (C): magnified loops in the low Hc field): (a) S1, (b) S2, (c) S3, (d) S4, (e) S5, and (f) S6.

DSHP show weak ferromagnetic behavior with saturation magnetization (Ms), remanent magnetization (Mr), and coercivity (Hc) of ca. 4.3 emu/g, 1.4 emu/g, and 83.8 Oe, respectively (see Figure S3, Supporting Information). The low Ms and Mr values can be attributed to the presence of phosphorus and the noncrystalline nature of the NiP shell. Compared with the glass−NiP DSHP, the glass−NiP−CoFeP TSHP obtained by the further assembly of the CoFeP shell exhibited enhanced ferromagnetic property. The hysteresis loops of samples S1−S6 obtained at room temperature are shown in Figure 7A. It can be inferred from the hysteresis loops that all the samples are magnetically soft at room temperature. To give a clearer observation of the central part of the hysteresis loops, the enlarged views in low Hc field are also presented in Figure 7B,C. Moreover, the changes of the Ms and Hc values over the mole ratios of Fe^{2+} ($Fe^{2+}/(Co^{2+} + Fe^{2+})$) in the reaction system are summarized in Figure 8.

It can be seen that, at lower mole ratios, the Ms value increased but the Hc value reduced with the increased mole ratio. The results were reasonable if we took into consideration that iron possesses better magnetic properties than other iron group metals and increasing the amount of Fe in the alloys can obviously improve the magnetic properties of NiFeP or CoFeP ternary alloys.[18,21] On the other hand, the reduced Hc value may be attributed to Fe substitution in Co lattice reducing the crystal anisotropy field. With the further increased mole ratios, the Ms and Hc values also change in an opposite manner: the

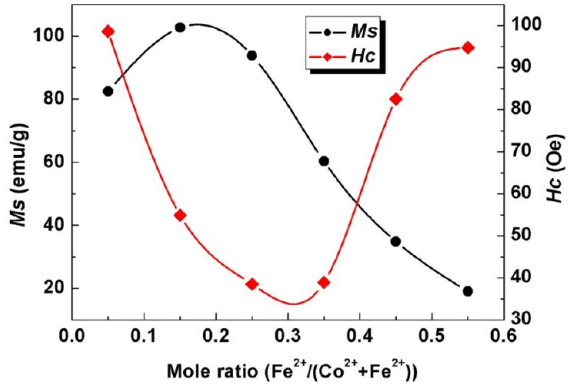

Figure 8. Changes of saturation intensity (Ms) and coercive force (Hc) of the glass−NiP−CoFeP TSHP obtained at various mole ratios of Fe^{2+} ($Fe^{2+}/(Co^{2+} + Fe^{2+})$) in the reaction system.

Ms value was reduced gradually while the Hc value increased with points of inflection at mole ratios of ca.0.2 and ca.0.3 on the Ms−mole ratio curve and the Hc−mole ratio curve, respectively. This may be attributed to the reduced density and CoFeP shell thickness, which led to the decreased magnetic CoFeP phase content of the TSHP and enhanced shape anisotropy.[22−24]

To eliminate the influence of real density on the magnetic properties of the products, TSHP with the same density were needed for the VSM measurement. Exploratory experiments

dx.doi.org/10.1021/am3026344 | ACS Appl. Mater. Interfaces 2013, 5, 989−996

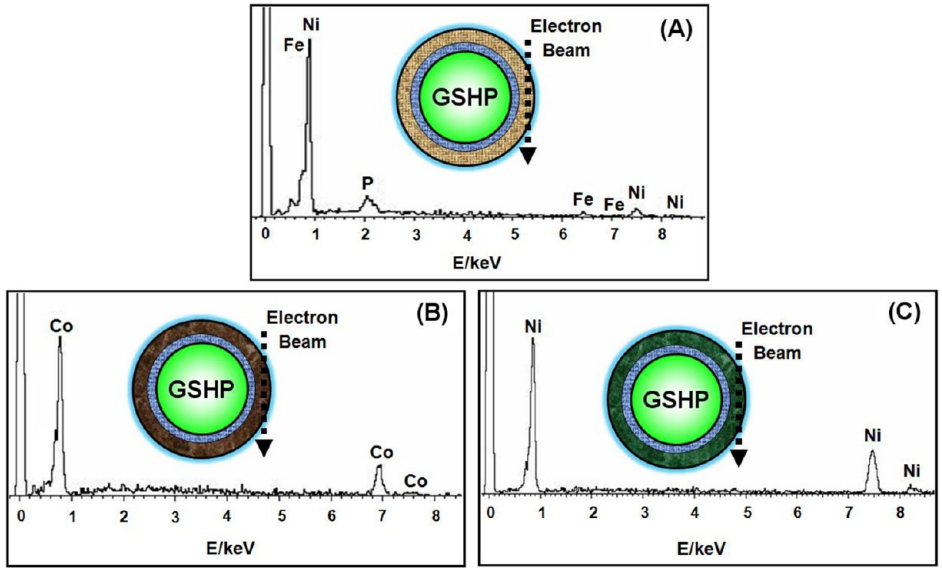

Figure 9. EDX spectra of various MSHP taken by passing the beam through the outermost shell. The inner and middle shells of these microspheres are silicate glass and NiP, respectively (the same as the glass−NiP−CoFeP MSHP), but the outermost shells are Ni−Fe−P alloy, Co, and Ni for panels (A), (B), and (C), respectively.

with tailored reaction system component, reaction time, or circle have been carried out, aimed at tuning the shell thickness and real density of the products. The results confirmed that it was possible to tailor the density of the products through the control of the above-mentioned reaction factors. However, more detailed work is still needed, and further study is underway to investigate the strategy for fine density and shell thickness control. Moreover, the results of exploratory experiments also revealed that, in addition to CoFeP shell, the NiP shell (assembled by little granules) also possessed catalytic activity for the formation and directed assembly of other metal or alloy shells. As the EDX spectrum of Figure 9 exhibited, TSHP with the same glass and NiP shells as the glass−NiP−CoFeP TSHP but different outmost shells can be prepared through the same strategy mentioned above (with a properly monitored reaction system). As shown in Figure 9, TSHP with the outmost shell composed of NiFeP alloy, metallic cobalt, and nickel have been prepared. It can be expected that, by properly designing and controlling the component of the reaction system and the reaction solution, the fabrication strategy reported here holds the potential to be extended to the directed assembly of other shells. As for the properties, the multishell hollow particles (MSHP) may also possess tunable conduction and dielectrical and electromagnetic wave absorption properties in addition to magnetic properties. The systematic study of the controlled assembly of various shells to form MSHP with tailored composition, structure, morphology, and properties is still underway currently and will be reported in our future papers.

4. CONCLUSIONS

In summary, smooth and compact silicate glass shells, metallic granular nickel−phosphorus, and cobalt−iron−phosphorus shells were synthesized and assembled in the glass−NiP−CoFeP order through two-step spray drying−melting (for the glass shell) and subsequent catalyzed reduction in an aqueous system (for the metallic NiP and CoFeP shells), respectively. Thus, glass−metal−metal TSHP were successfully fabricated with low density and tunable magnetic properties. It is found that the coupling treatment of the GSHP by KH550 and the subsequent Ag seeds decoration were two key points for the formation of the NiP shells (which was the precondition for the formation and assembly of the CoFeP shells). Moreover, the results of the contrasting experiments in the assembly of the CoFeP shell demonstrated that it was possible to control the composition and structure of the outmost CoFeP shell by properly monitoring the component of the reaction system and further tailoring the magnetic properties of the final products. Exploratory experiments also revealed that, in addition to CoFeP shell, the NiP shell also possessed catalytic activity for the formation and directed assembly of NiFeP, Co, and Ni shells. It can be expected that, by properly designing and controlling the component of the reaction system and the reaction solution, the fabrication strategy reported here holds the potential to be extended to the directed assembly of other shells and preparation of MSHP with various composition and properties.

■ ASSOCIATED CONTENT

Ⓢ Supporting Information

The SEM images of the as-obtained quasi spherical precursor particles during the preparation of the particles with hollow core and glass shell (before smelting). The SEM images of the products obtained after NiP assembly on GSHP without coupling treatment before sensitization and activation. The curve depicting the field dependent magnetization at room temperature for the glass−NiP DSHP. This information is available free of charge via the Internet at http://pubs.acs.org/.

■ AUTHOR INFORMATION

Corresponding Author

*Tel/Fax: +86 10 82543690. E-mail: zgan@mail.ipc.ac.cn (Z.A.); jjzhang@mail.ipc.ac.cn (J.Z.).

Notes

The authors declare no competing financial interest.

■ ACKNOWLEDGMENTS

This work was supported by the National Natural Science Foundation of China (Project Nos. 51102248 and 50901083).

■ REFERENCES

(1) Wen, X.; Archer, L. A.; Yang, Z. *Adv. Mater.* **2008**, *20*, 3987−4019.
(2) Tang, F.; Li, L.; Chen, D. *Adv. Mater.* **2012**, *24*, 1504−1534.
(3) Hong, J.; Char, K.; Kim, B. *J. Phys. Chem. Lett.* **2010**, *1*, 3442−3445.
(4) Zhao, Y.; Jiang, L. *Adv. Mater.* **2009**, *21*, 3621−3638.
(5) Salgueirino-Maceira, V.; Correa-Duarte, M. A. *Adv. Mater.* **2007**, *19*, 4131−4144.
(6) Wei, S.; Wang, Q.; Zhu, J.; Sun, L.; Lin, H.; Guo, Z. *Nanoscale* **2011**, *3*, 4474−4502.
(7) Selvan, S.; Tan, T.; Yi, D.; Jana, N. *Langmuir* **2010**, *26*, 11631−11641.
(8) Yin, Y.; Rioux, R.; Erdonmez, C.; Hughes, S.; Somorjai, G.; Alivisatos, A. *Science* **2004**, *304*, 711−714.
(9) Liu, B.; Zeng, H. *Small* **2005**, *1*, 566−571.
(10) Li, J.; Zeng, H. *J. Am. Chem. Soc.* **2007**, *129*, 15839−15847.
(11) Grzelczak, M.; Vermant, J.; Furst, E.; Liz-Marzan, L. *ACS Nano* **2010**, *4*, 3591−3605.
(12) Chaudhuri, R.; Santanu, P. *Chem. Rev.* **2012**, *112*, 2373−2433.
(13) Caruso, F. *Adv. Mater.* **2001**, *13*, 11−22.
(14) Qi, X.; Gao, C.; Zhang, Z.; Chen, S.; Li, B.; Wei, S. *Int. J. Hydrogen Energy* **2012**, *37*, 1518−1530.
(15) Geleil, A.; Hall, M.; Shelby, J. *J. Non-Cryst. Solids* **2006**, *352*, 620−625.
(16) Li, X.; Duan, Y.; Zhao, Y.; Zhu, L. *Prog. Nat. Sci.* **2011**, *21*, 392−400.
(17) Dong, D.; Chen, X.; Xiao, W.; Yang, G.; Zhang, P. *Appl. Surf. Sci.* **2009**, *255*, 7051−7055.
(18) An, Z.; Zhang, J.; Pan, S. *Appl. Surf. Sci.* **2008**, *255*, 2219−2224.
(19) Wang, S. *Surf. Coat. Technol.* **2004**, *18*, 372−376.
(20) Xie, G.; Wang, Z.; Cui, Z.; Shi, Y. *Carbon* **2005**, *43*, 3181−3194.
(21) Kim, S.; Kim, S.; Ahn, J.; Kim, K. *J. Magn. Magn. Mater.* **2004**, *271*, 39−45.
(22) Diandra, L.; Reuben, D. *Chem. Mater.* **1996**, *8*, 1770−1783.
(23) Guirado-Lopez, R.; Aguilera-Granja, F. *J. Phys. Chem. C* **2008**, *112*, 6729−6739.
(24) Seto, T.; Akinaga, H.; Takano, F.; Koga, K.; Orii, T.; Hirasawa, M. *J. Phys. Chem. B* **2005**, *109*, 13403−13405.